Recombination centers in $GaAs/Al_{0.4}Ga_{0.6}As$ heterostructures investigated by optically and electrically detected magnetic resonance

T. Wimbauer, M. S. Brandt, M. W. Bayerl, N. M. Reinacher, and M. Stutzmann
Technische Universität München, Walter Schottky Institut, Am Coulombwall, D-85747 Garching, Germany

D. M. Hofmann
I. Physikalisches Institut, Justus-Liebig-Universität Gießen, Heinrich-Buff-Ring 16, D-35392 Gießen, Germany

Y. Mochizuki and M. Mizuta
Fundamental Research Laboratories, NEC Corporation, 34 Miyukigaoka, Tsukuba, Ibaraki 305, Japan
(Received 24 December 1997)

Using optically and electrically detected magnetic resonance (ODMR and EDMR, respectively), recombination in a $GaAs/Al_{0.4}Ga_{0.6}As$ heterostructure is studied. ODMR performed at 35 GHz shows the presence of Ga interstitials in a GaAs quantum well codoped with Si and Be. Depending on the contacts used, EDMR (performed both at 9 and 34 GHz) is able to detect surface defects, intrinsic defects (Ga interstitial and As_{Ga} antisite) as well as the Cr^{4+} transition-metal impurity. The location of the paramagnetic states in the heterostructure was determined with EDMR using light of different absorption length for the selective excitation of photoconductivity, combined with a phase shift analysis of the different EDMR signals with respect to the modulation reference. The temperature and microwave power dependence of the EDMR signal amplitude is discussed, providing guidelines for the experimental conditions needed to perform EDMR on GaAs. Finally, using *X*-band and *Q*-band detection, the defect parameters (*g*-factor and hyperfine constants) for the Ga interstitial are determined to $g=2.006$, $A_{69}=0.048\ cm^{-1}$, and $A_{71}=0.061\ cm^{-1}$. These results are compared to previous observations. [S0163-1829(98)01232-6]

I. INTRODUCTION

Among the large variety of experimental methods to characterize semiconductors, magnetic resonance techniques are probably the most powerful to obtain detailed information on point defects in these materials. In general, electron paramagnetic resonance (EPR) experiments allow one to resolve various interactions of the defect electron(s), such as fine-structure, hyperfine, and ligand-hyperfine interactions. From the data, one can obtain knowledge about the chemical nature of the defect, whether it is a simple point defect or a complex (defect symmetry), the charge state of the defect (spin state), and, last but not least, the defect concentration. The major problem for the application of EPR to epitaxial layers or quantum-well structures is the sensitivity limit of the method. In epitaxial systems, the reduced size of the sample volume, a few micrometers for layers or even only a few nanometers in the case of quantum wells, pushes the number of defects to be detected below the limit of about 10^{11} spins per Gauss linewidth. Thus, most investigations on epitaxial structures make use of optically detected magnetic resonance (ODMR), in which the defects are studied via resonant changes of the magnetic dichroism or the photoluminescence intensity.[1] Besides a much higher sensitivity, ODMR has further advantages in view of selectivity. As quantum wells or other low-dimensional structures typically show specific radiative recombinations, the magnetic resonance features can be related to these structures by spectrally resolved ODMR experiments. In addition to the conventional EPR, ODMR enables us to study optically created paramagnetic species like excitons, which are not present in thermal equilibrium.

Another approach to make magnetic resonance experiments compatible with modern semiconductor structures is electrically detected magnetic resonance (EDMR).[2,3] The principle of EDMR is the modification of an electrical current through the sample, via spin-dependent recombination or hopping processes. Under magnetic resonance conditions, a resonant current change is induced, which is detected in the EDMR experiment. A particular advantage of EDMR is that the influence of defects on the properties of actual electronic and optoelectronic devices can be studied, which is in general not possible with ODMR or classical EPR. As far as sensitivity is concerned, EDMR has the same high potential as ODMR, where magnetic resonance of a single molecule has been demonstrated.[4,5] In view of selectivity, the potential of the EDMR has been explored much less. Most EDMR experiments reported so far deal with defects in bulk semiconductors, thin films, or simple p/n diode structures.[6,7] While such experiments have been very successful for semiconductors with indirect band gaps, such as Si,[3] SiC,[8] and GaP,[9] experiments on direct band-gap semiconductors are rare, with GaN light-emitting diodes[8,10] and a study of low-temperature GaAs (Ref. 8) being the only examples known to the authors. It was conventionally assumed that, due to the short lifetimes of excited carriers in direct band-gap materials, spin-flip rates beyond the capabilities of classical EPR spectrometers would be needed to achieve a reasonable resonant change of the recombination rate, the detection limit

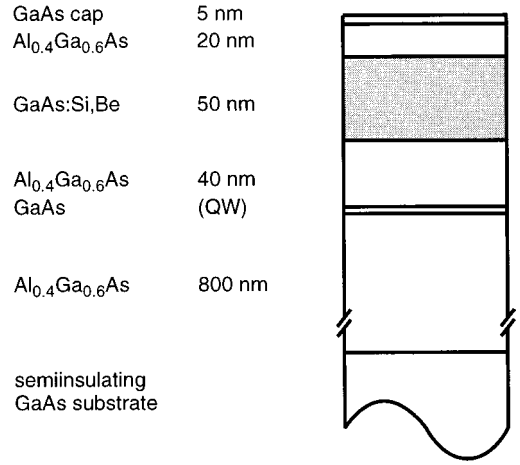

FIG. 1. Layer sequence of the sample investigated. The 50-nm-thick GaAs layer is codoped with Si (1×10^{16} cm^{-3}) and Be (3×10^{16} cm^{-3}) in order to get a slow DAP recombination for the ODMR study.

being a relative change of the conductivity $\Delta\sigma/\sigma$ of about 10^{-7}.

However, in this paper we demonstrate that GaAs heterostructures can be studied with EDMR achieving the same sensitivity as previously only known for group-IV semiconductors. In addition, we show that the method is sensitive enough to resolve defects in III-V quantum-well structures. Changing the wavelength of the excitation light, a selectivity to the location of the specific defects in the different layers of the complex structure is achieved, complementary to what is obtained by ODMR. To this end, we have performed a comparative ODMR and EDMR study of a GaAs/$Al_{0.4}Ga_{0.6}As$ heterostructure on a semi-insulating GaAs substrate. The ODMR results show the presence of Ga interstitial defects in a 50-nm-wide GaAs ''quantum well.'' In the EDMR experiments, the interstitial as well as three additional defects were observed. Variations of the contact properties and the experimental parameters allow us to separate these signals and to identify them as surface-related defects and defects located in the substrate (Cr^{4+} and arsenic antisite defects).

II. EXPERIMENT

A. Sample structure

The layer structure of the GaAs/$Al_{0.4}Ga_{0.6}As$ heterostructure studied here is shown in Fig. 1. To have a slow recombination channel that is more easily accessible to ODMR studies, a 50-nm GaAs film codoped with both Si (1×10^{16} cm^{-3}) and Be (3×10^{16} cm^{-3}), denoted as the GaAs:*D*,*A* layer, was sandwiched between $Al_{0.4}Ga_{0.6}As$ cladding layers. The original purpose of this design was to study defects introduced during the dry-etching processes, so the GaAs:*D*,*A* layer was positioned within the near-surface region where most of the damage is expected.[11] Throughout the whole structure, it is only this GaAs:*D*,*A* layer that emits at the near-band-gap energy of GaAs. Therefore, by monitoring photoluminescence (PL) in this energy range, the region probed by spin resonance (ODMR) can be limited to this 50-nm-thick layer.

As mentioned, the codoping was employed because of lifetime considerations. In order to perform ODMR measurements, in which one monitors a spin-flip-induced perturbation in the population of radiative species, it is convenient to use a luminescent process with small decay rates. In donor-acceptor pair recombination, electrons and holes recombine via tunneling between the trapped impurity sites and the small overlap of the carrier wave functions yields radiative lifetimes of the order of 10^{-7} s. A single quantum well was also inserted at a deeper location (115 nm from the surface) in order to avoid a high level of carrier injection into the GaAs:*D*,*A* layer.

The epitaxial film was grown by molecular-beam epitaxy (MBE) onto the (001) surface of a semi-insulating GaAs substrate. The substrate temperature and V/III flux ratio were 580 °C and 6.3, respectively. The doping concentration of the GaAs:*D*,*A* layer cannot be easily checked from a direct measurement since the layer was codoped. Instead, in order to calibrate the dopant-cell temperatures, we repeated MBE growth of singly Si- and Be-doped GaAs for several times, which were then characterized by Hall measurements, just prior to the growth of the codoped sample.

B. ODMR setup

ODMR was measured with a spectrometer consisting of a 4-T superconducting magnet (modified Oxford MD-4) and a 35-GHz microwave system. The cylindrical resonator had a wall-less concentric annular-ring structure to allow optical access.[12] During the measurements, the sample and the resonator were immersed in pumped liquid He (1.6 K). The microwave power ($\leqslant$100 mW) was supplied by a GaAs Gunn diode, whose frequency was automatically stabilized to seven digits by using a source-locking frequency counter.

Luminescence was excited by an Ar^+ laser (488 nm, 1 mW/cm^2). The emission was collected and guided to a Si photodiode (Hamamatsu Photonics), whose output was fed to a current amplifier. (When we used a Ge detector instead, the monitored luminescence was dominated by a deep-level emission that was found to give rise to a strong triplet ODMR thereby masking the spin resonance signal from the GaAs:*D*,*A* region.) Into the optical path, we inserted a glass filter to extract the luminescence whose wavelength was longer than 810 nm. ODMR was measured with lock-in detection by chopping the applied microwave power while the static field was swept. The typical chopping frequency was 1.2 kHz.

C. EDMR setup

EDMR was performed both at 9 and at 34 GHz. The 9-GHz EDMR spectrometer consists of a standard EPR spectrometer (Bruker ESP 300), equipped with a rectangular TE_{102} resonator. A Keithley source measure unit 237 was used as a low-noise voltage source and lock-in technique for sensitive detection of either the magnetic field or the microwave amplitude modulated signal. The measurement temperature could be varied with a helium flow cryostat (Oxford ESR 900) from 4 to 300 K and the sample was illuminated with a 100-W tungsten lamp in combination with a KG3 heat filter.

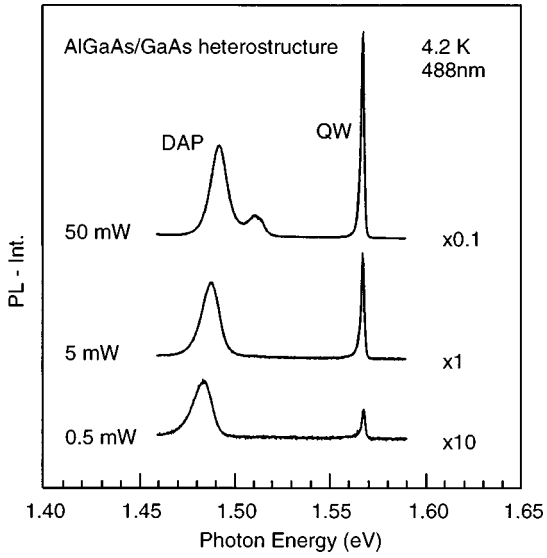

FIG. 2. Photoluminescence spectra taken at different excitation powers (the power data in the figure refer to the actual incident power on the sample). At weak excitation the shallow DAP process (1.48 eV) is dominating. With increasing power the peak shifts to higher energies due to a change in the relative contributions of DAP and free-to-bound transitions. At 1.567 eV the quantum-well luminescence is seen.

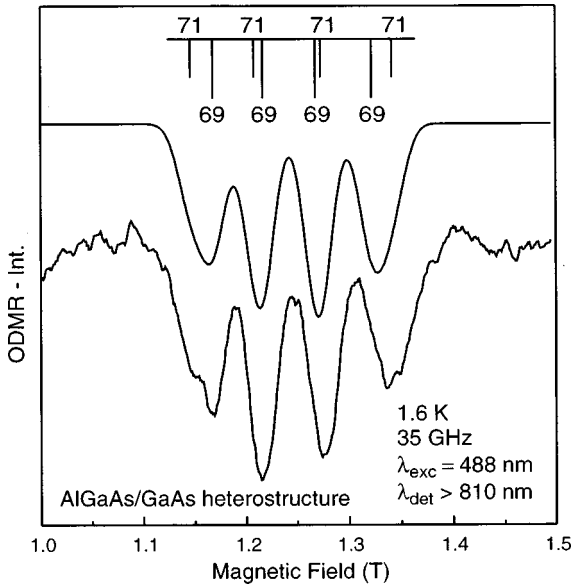

FIG. 3. Experimental and simulated Q-band ODMR spectra of the Ga interstitial. For the calculations a g value of $g=2.006$ and hyperfine constants of $A_{69}=0.048$ cm^{-1} and $A_{71}=0.061$ cm^{-1} have been used. The calculated line positions are indicated by vertical lines, proportional to the natural abundances of the Ga isotopes.

For EDMR experiments at 34 GHz, a spectrometer consisting of a HP 83640A microwave synthesizer, a microwave power amplifier, and a cylindrical resonator (Bruker ER 5106 QT) immersed in a helium bath cryostat (Oxford CF 935) was employed. The synthesizer and the amplifier allow the use of the spectrometer over the whole *K*a-band (26.5–40 GHz) with a power of more than 200 mW. The same modulation, detection and illumination schemes are used at 34 GHz as at 9 GHz.

III. RESULTS

A. ODMR

We first present the ODMR data. Since our sample has a special structure that allows an ODMR study in a specific depth region, the result serves as a good reference for the EDMR study, especially in relating defects with specific regions (probed layers) within the multilayer structure.

Figure 2 shows the photoluminescence spectra taken at 4.2 K. When excitation is weak, the near-band-edge emission is dominated by the shallow donor-acceptor process (DAP). Additionally, another luminescence was observed at 1.567 eV (above the band-gap energy of GaAs), which is due to the single quantum well and not related to the GaAs:D,A layer. In the present sample, photoluminescence due to the $Al_{0.4}Ga_{0.6}As$ cladding layers was not detected. Deep-level luminescence bands were also observed at 1.41, 1.36, and 0.8 eV, respectively. The intensities of these emissions were only comparable to or smaller than that of the first phonon replica of the shallow DAP line. Although it is not clear from which layer of the epitaxial film these emissions originate, they hardly play an important role in the ODMR experiments.

In Fig. 2, it is seen that the peak at 1.48–1.49 eV shifts to lower energies as the excitation becomes weaker. This shift is attributed to a change in the relative contributions of DAP and free-to-bound (free electron to acceptor) transitions, and also to the peak shift within the DAP transition. In fact, we have checked the contributions of these two mechanisms by measuring the wavelength dependence of optically detected cyclotron resonance, whose signal goes through a sign reversal between the DAP and free-to-bound transitions.[13] In the topmost trace, where the excitation was strong, exciton-related emissions were also detected. However, the excitation intensity employed in our ODMR experiment (≈ 1 mW/cm^2) was even smaller than that for the lowermost spectrum, so we conclude that the DAP emission due to the intentionally doped shallow impurities (within the GaAs:D,A layer) was the dominant luminescence contribution in the ODMR experiment.

The ODMR spectrum is shown in Fig. 3. When recording the spectrum, we inserted an optical long-pass filter with the cutoff at 810 nm (1.53 eV). Since we used a Si detector, the luminescence monitored during the experiment consists of the shallow DAP and the two deep-level (1.41 and 1.36 eV) bands, with the former emission being dominant. In fact, we checked that the feature of Fig. 3 is indeed due to the shallow DAP process by subtracting the ODMR spectrum with 840-nm cutoff from that with 810-nm cutoff.

The sign of the ODMR was negative: the intensity of the shallow DAP luminescence decreased at the spin resonance. This means that the observed defect is likely to act as a shunt path for the radiative process. Therefore, it is suggested that the defect is a residual nonradiative center that was incorporated during the MBE growth. The spectrum consists of four lines, in which the central two lines are narrower and larger than the outer two. Assuming that the four-line spectrum is due to a hyperfine interaction with Ga nuclei ($I=3/2$), the natural abundance ratio for ^{69}Ga and ^{71}Ga can explain the observed spectrum quite well as seen in Fig. 3. The parameters (g values and hyperfine constants) are in fact in agree-

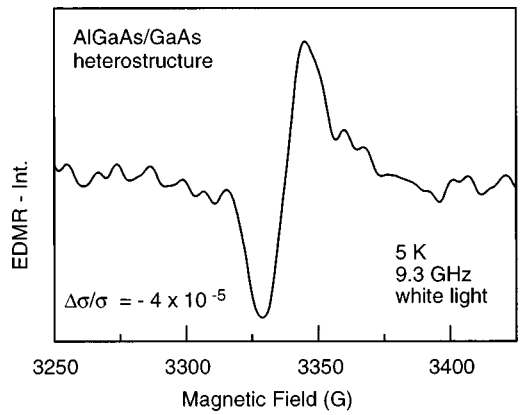

FIG. 4. EDMR spectrum of the surface dangling-bond-related defect. For the investigation, silver paste contacts on top of the GaAs cap layer were used in order to restrict the current to the cap layer.

ment with those of various Ga interstitials, as discussed below. As is clear from the foregoing discussions, the region in which we detected the Ga-interstitial defects is the 50 nm-thick GaAs:*D*,*A* region.

We have also performed ODMR measurements by monitoring the 0.8-eV luminescence using a cooled Ge detector. In this case, a PL-enhancing ODMR, which consists of multiple lines over a wide magnetic field range, was observed. The feature, to some extent, is analogous to the previously reported deep triplet ODMR in GaAs but full details of the spectra were not in agreement.[14,15] Anyway, since the spatial location of the radiative species for the 0.8-eV band is not conclusive within the multilayered structure, it is difficult to determine the origin of the enhancing ODMR.

B. EDMR

1. Nonalloyed Ag contacts

We now turn to the investigation of spin-dependent recombination via conductivity measurements. The observed spin-dependent photoconductivity signals strongly depend on the properties of the electrical contacts used for the experiments. The most simple were made by applying silver paste on top of the sample. In order to create photoexcited carriers, the sample was illuminated with the unfiltered light of a halogen lamp (''white light'' conditions). Using this illumination, the signal shown in Fig. 4 was detected at 5 K. The derivative shape of the resonance is caused by the magnetic-field modulation used for the experiment. The signal amplitude is of the order of $\Delta\sigma/\sigma \approx -4\times10^{-5}$, for microwave powers of 400 mW. Neither a saturation nor an anisotropy of the resonance could be observed. Its field position corresponds to $g=2.001$ and the peak-to-peak linewidth is $\Delta H_{pp}=18$ G. The g value close to the free electron value is not a very specific defect feature, but the halfwidth of the resonance is surprisingly small for a defect in GaAs or $Al_{0.4}Ga_{0.6}As$, as all nuclei of the host carry nuclear spin and thus interact with the defect electron via hyperfine interaction. As discussed below, this leads to magnetic resonance linewidths that typically are an order of magnitude higher for defects in GaAs and $Al_{0.4}Ga_{0.6}As$ compared to the defect observed here.

However, Emanuelson *et al.*[16] reported the observation of a defect with very similar properties by EPR in a study of $Al_{0.4}Ga_{0.6}As$/GaAs heterostructures. The signal was observable in samples that had been subject to a surface treatment by reactive ion etching. After a removal of the damaged surface layer by a wet etching process the EPR line disappeared. This indicated that the signal originated from the surface layer, which led to the attribution to surface dangling-bond-related defects.

Our results support these conclusions, as we expect that due to the silver paste contacts the current through the sample is mostly flowing in the uppermost GaAs cap layer and thus being dominantly sensitive to surface-related defects. In the previous EPR investigation it was shown that the presence of this dangling-bond defect causes an increase of the carrier scattering rate determined by Shubnikov–de Haas measurements. However, the observation of the dangling-bond defects in EDMR indicates that they also act as recombination centers. Additionally, our results suggest that this type of defect is not specific for the growth technique of the sample, metal-organic vapor-phase epitaxy (MOVPE) in the case of Ref. 16 or MBE in our case, and that chemical reactive species are unlikely to be directly involved in the defect structure. The MBE samples used in our investigation have not been subject to a reactive ion etching process, but instead were kept in air for several months before the EDMR investigations.

2. Alloyed In contacts

In a second step, indium contacts (alloyed at 480 °C for 1 min) were used in order to achieve electrical contact to all regions of the layered structure. Using these contacts and illuminating the sample with white light the spectrum shown in Fig. 5 was observed. Microwave power modulation was used in these experiments, leading to nonderivative lineshapes. The amplitude of the dominating central signal is $\Delta\sigma/\sigma=-8\times10^{-5}$. The sign has been carefully checked using modulation at very low frequencies to avoid additional phase shifts caused by the detection circuit, as discussed below. The central signal is well described by a Gaussian, has a g value of $g=1.99$ and a full width at half maximum of 200 G. These resonance parameters are consistent with Cr^{4+} ($3d^2$, $S=1$) (Ref. 17) located in the Cr-doped semi-insulating GaAs substrate, a clear indication that electrical contact was made to the substrate by the alloying procedure. In order to describe the low-field and high-field parts of the experimental spectrum in Fig. 5, the well-known EPR parameters of the arsenic antisite defect As_{Ga} were used (g factor $g=2.047$, hyperfine constant $A=0.089$ cm^{-1}, nuclear spin $I=3/2$ of As).[18] The simulation of As_{Ga} in Fig. 5 shows that the two outermost resonances of the experimental spectrum can indeed be explained by the existance of the arsenic antisite defect, which is most likely also located in the semi-insulating GaAs substrate. Further including the Ga interstitial Ga_i, as discussed below, a better agreement with the experimental spectrum can be achieved with respect to the shoulders localized more closely to the central high intensity line, a strong indication that the Ga interstitial defect in the codoped layer also acts as a recombination center for the photoexcited carriers. We will show in the next section that the resonances due to the Ga interstitial can also be experimentally separated using EDMR.

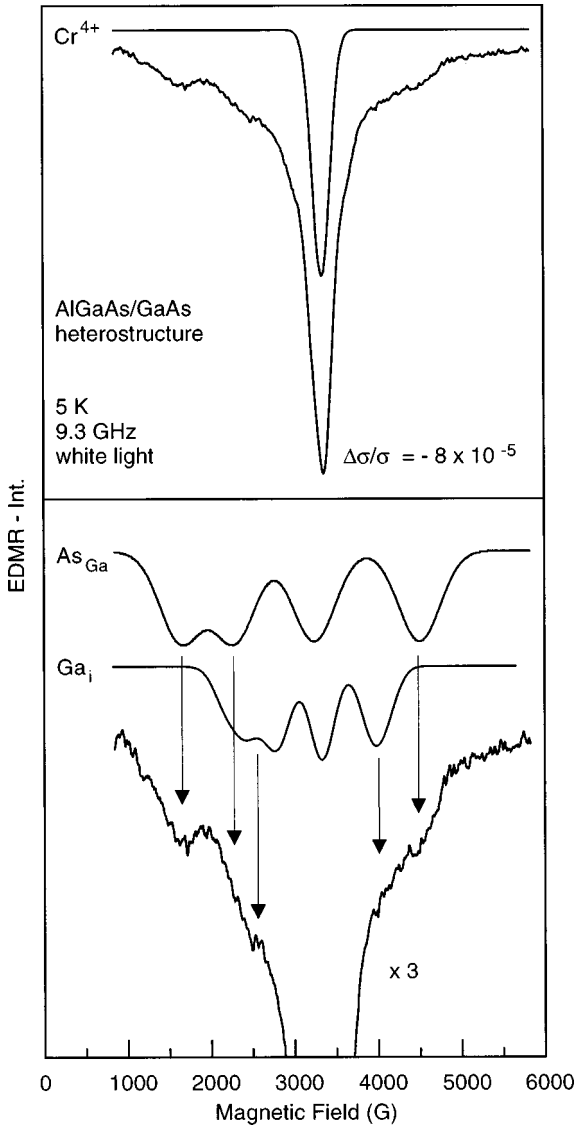

FIG. 5. EDMR spectrum using alloyed In contacts. The In contacts allow a current flow in deeper layers of the sample. The decomposition of the superimposed resonances into Cr^{4+}, As_{Ga}, and Ga_i is shown. Cr^{4+} as well as As_{Ga} are located in the substrate whereas the Ga_i is located in the codoped GaAs layer.

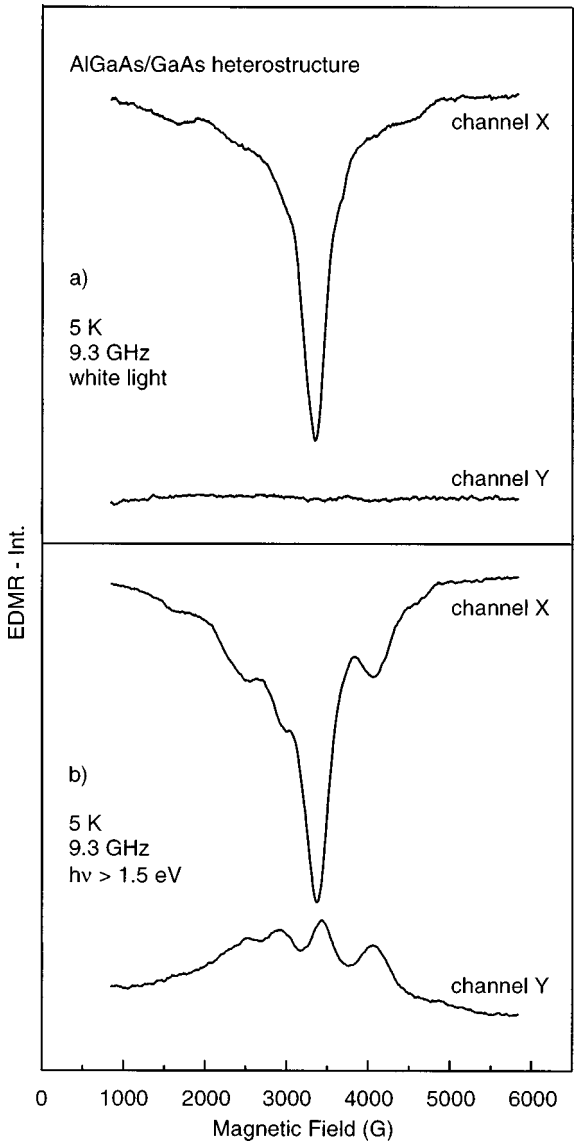

FIG. 6. Experimental separation of the Ga_i resonances from the substrate signals. (a) Under illumination with white light, all signals have the same phase delay with respect to the modulation, no signal in channel Y shifted by 90° with respect to channel X is observed. (b) In the case of inhomogeneously absorbed light only ($h\nu \geqslant 1.5$ eV), the substrate signals and the signals from the codoped layer have different phase delays with respect to the modulation, the Ga_i signal can be isolated in channel Y. See text for details.

3. Phase shift analysis

ODMR can be made selective by monitoring resonant changes of certain photoluminescence lines and thereby correlating the defect to certain radiative or shunt processes. We show here that EDMR can be used in a complementary way to obtain spatial information concerning the position of defects in different layers of a structure by changing the carrier concentration in the layers. A clear separation of the signals from the GaAs substrate and the codoped layer is achieved by comparing the EDMR response of the heterostructure illuminated with inhomogeneously absorbed light above the band gap of GaAs ($h\nu > 1.5$ eV) to the EDMR response when illuminating the sample with white light including homogeneously absorbed light with $h\nu < 1.5$ eV. The sample was painted black on the substrate side, so that illumination only took place through the heterostructure. The results of these measurements are shown in Fig. 6. In the case of homogeneous illumination (white light, upper part of Fig. 6), by changing the phase difference α between modulation and detection it was possible to ''shift'' all resonances into channel X of the two-phase lock-in amplifier with no resonance in the quadrature channel Y. This means that all resonances exhibited the same phase shift with respect to the modulation. In contrast, under inhomogeneous illumination with $h\nu > 1.5$ eV (lower part of Fig. 6), a detection of all signals in only one channel was impossible. Instead, in this case it is possible to find a phase shift α_{sub} between modulation and detection that allows the separation of the isolated Ga_i resonances originating in the codoped layer (channel Y) from the sum of all resonances (Ga_i, Cr^{4+}, and As_{Ga}) (channel X).

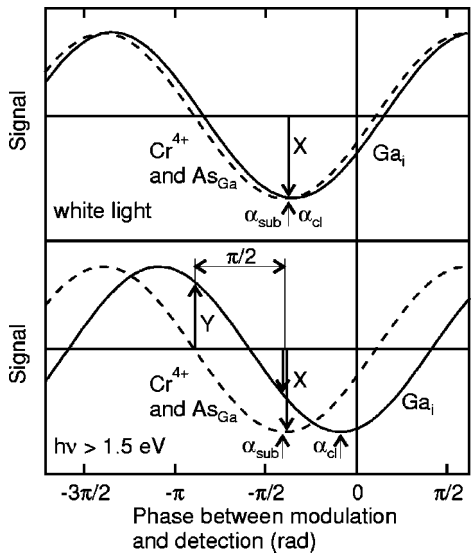

FIG. 7. Amplitudes of the signals from the different sample layers as a function of the phase between modulation and detection for the two different illumination schemes.

These experimental facts are illustrated in Fig. 7, which shows the amplitudes of the signals from the codoped layer (solid curve) and the substrate signals (dashed curve) as a function of the phase between modulation and detection. It is seen that a phase shift analysis[19,20] is possible if the signal phase α_{cl} of the resonance originating from the codoped layer differs from the corresponding α_{sub} of the substrate as is the case when $h\nu > 1.5$ eV. By setting the phase between the modulation and detection channel X equal to α_{sub}, all resonances appear in channel X, the signals from the substrate in full intensity (dashed line in Fig. 7) and those from the codoped layer (straight line) in reduced intensity, whereas in the quadrature channel Y the substrate signal amplitude is completely suppressed and the isolated signal amplitude from the codoped layer appears, however with reduced intensity and inverted sign. In this way, the EDMR spectra of the isolated Ga_i resonances as shown in Fig. 12 (upper part) could be recorded. In addition to the 9 GHz results described above, similar EDMR experiments were performed at 34 GHz using the identical sample and illumination conditions, giving rise to the Q-band EDMR spectrum of the Ga_i (lower part of Fig. 12) which has a signal/noise ratio similar to the ODMR results shown in Fig. 3.

In principle, there can be several contributions to the observed phase shift of the signal with respect to the modulation: delays in the modulation and detection circuits, in particular due to amplifiers, and relaxation processes of the electronic transport through the sample. The overall detection system includes several amplifiers such as the driver of the pin diode used for microwave modulation and the preamplifier of the lock-in. However, their influence should be a constant contribution to both α_{cl} and α_{sub} and should not induce a relative phase shift. Details of the sample, including the particular way contact is made to it, could be the origin of the phase shift. In order to clarify this contribution, the equivalent circuit of the EDMR setup is shown in Fig. 8. The essential parts are two photoresistors, formed by the substrate R_{sub}, the co-doped layer R_{cl}, the capacitance of the

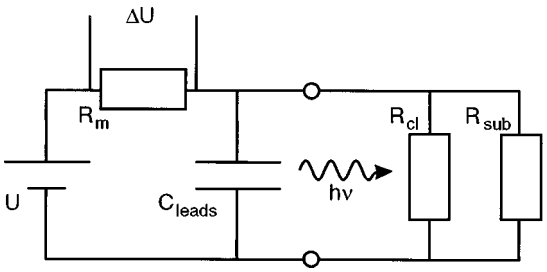

FIG. 8. Equivalent circuit of the EDMR setup containing two photoresistors formed by the substrate R_{sub}, the codoped layer R_{cl}, the capacitance of the leads C_{leads}, the resistor R_M, and a constant voltage source.

leads C_{leads}, the resistor R_m as current-to-voltage converter, and a constant voltage source. Because of the spin-dependent effect, the resistors corresponding to the layers contain an oscillating component under magnetic resonance conditions; hence, they can be written in the form $R = R_0 + R_1 \sin(\omega_{mod} t)$. In the case of a homogeneous sample described by a single resistor R, standard network analysis under small signal approximation yields

$$\Delta U = U \frac{R_1 R_m}{(R_0 + R_m)^2 \sqrt{1 + \left(\omega_{mod} C_{leads} \frac{R_m R_0}{R_m + R_0} \right)^2}} \tag{3.1}$$

for the voltage ΔU detected by the lock-in amplifier and a phase shift between modulation and detection given by

$$\alpha = \frac{\pi}{2} + \arctan\left(\omega_{mod} C_{leads} \frac{R_m R_0}{R_m + R_0} \right). \tag{3.2}$$

The applicability of these equations has been confirmed experimentally for simple photoconductive samples using different light intensities to change R. When the single photoconductor R is replaced by $R_{cl} = R_{cl0} + R_{cl1} \sin(\omega_{mod} t)$ and $R_{sub} = R_{sub0} + R_{sub1} \sin(\omega_{mod} t)$, Kirchhoff's rules predict $\alpha_{cl} = \alpha_{sub}$ for all values of R_{cl0} and R_{sub0}. A relative phase shift between α_{cl} and α_{sub} can only be accounted for by a simple RC network introducing an additional capacitive element. This could in principle be caused by the capacitive coupling of the two layers through the $Al_{0.4}Ga_{0.6}As$ spacer (which has a capacitance of ≈ 1 nF), if at least one of the contacts to the two layers has a significant contact resistance or is non-Ohmic, which is is not the case for In contacts used. Indeed, slightly modulating the light under the different illumination schemes and detecting the photoresponse with the setup shown in Fig. 8 has not led to any significant phase shifts between modulated light intensity and photocurrent.

The observed relative phase shift can therefore only arise due to changes in the microscopic processes leading to $R_{sub} = R_{sub0} + R_{sub1} \sin(\omega_{mod} t + \alpha_{sub})$ and $R_{cl} = R_{cl0} + R_{cl1} \sin(\omega_{mod} t + \alpha_{cl})$. Delays in the recombination causing such phase shifts can occur due to recombination life times or spin-relaxation times. However, recombination times (the

intentionally slow DAP process in the codoped layer has a recombination time already as fast as 1 μs) are much too fast to explain the observed phase shift of 40° at 1-kHz modulation frequency. The influence of slow recombination would also have been detected in the photoconductivity experiments under modulated light, and therefore can also be excluded experimentally. This leaves changes in the spin-relaxation processes as the only plausible explanation, as has also been concluded for *a*-Si:H, where a similar phase shift analysis can be performed.[19,20]

Very few data are available on the spin relaxation, in particular the spin-lattice relaxation time T_1, in GaAs. In particular, it has been found that T_1 for the As_{Ga} antisite can vary over orders of magnitude depending on the defect concentration and at low temperatures can reach seconds in high-quality materials such as the substrate explored in this study.[21] However, high concentrations of photoexcited carriers reduce such long times significantly. This causes the observed changes of the phase shift: Under both illumination schemes a high concentration of charge carriers is created in the codoped layer so that the spin-lattice relaxation is so fast that upon switching of the microwave power, the relaxation back to equilibrium is not delayed by a long T_1 and, therefore, the conductivity relaxes instantaneously so that no phase shift is observed. In the substrate, however, the carrier concentration is changed drastically upon changes of the illumination scheme. Using white light, a high carrier concentration in the substrate is achieved as well, leading to a short T_1 of the defects observed and no additional phase shift. Using light that is strongly absorbed in the codoped layer only, very little carriers are excited in the substrate, leading to a long T_1 and an appreciable relaxation time, which is translated into the additional phase shift observed in Fig. 8. It is important to note that the carrier concentration seems to have the identical effect on both the Cr^{4+} and the As_{Ga} defects, since no phase shift between these signals could be resolved.

Using this dependence of T_1 on the carrier concentration, a spatial assignment of the defects observed to different layers in a multilayer sample can be achieved. However, as will be discussed in the following, it is important to keep T_1 long enough to allow the successful detection with EDMR, which, in view of the results reported here requires low illumination intensities when high-quality GaAs is to be investigated.

4. Dependence of the EDMR amplitude on experimental conditions

Having demonstrated that EDMR can be a very useful tool to detect various types of recombination centers in GaAs, it is now interesting to establish the experimental conditions for this detection. Several aspects are important, such as the temperature range over which EDMR can be applied to study GaAs, or whether the defect density can be estimated from the signal amplitude $\Delta\sigma/\sigma$. While detailed experiments concerning these issues are currently performed on neutron-irradiated bulk GaAs, some information can already be obtained from the present investigation on GaAs heterostructures.

Figure 9 shows the temperature dependence of the dominant Cr^{4+} EDMR signal amplitude measured with the *X*-band spectrometer using low-intensity illumination. For

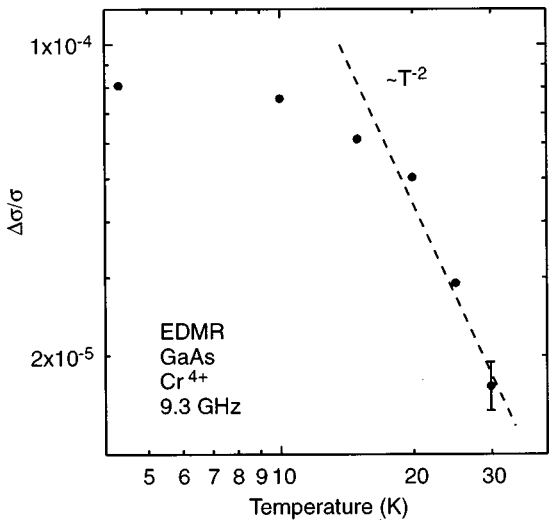

FIG. 9. Temperature dependence of the Cr^{4+} EDMR signal amplitude. When relaxation becomes so fast that no saturation can be reached with the microwave power available, the signal amplitude is drastically reduced.

temperatures up to 10 K, nearly no temperature dependence is observed. However, above 10 K, a very strong reduction of the signal amplitude is evident from Fig. 9. In order to understand this behavior, we briefly review the basic models proposed for a quantitative description of the EDMR signal amplitude. The original Lepine model[3] describes the spin-dependent process as a result of the interaction of the spin-polarized ensembles of conduction electrons and defects, giving rise to a $\Delta\sigma/\sigma \propto [g\mu_B H/(kT)]^2$ dependence. Such a T^{-2} dependence as sketched in Fig. 9, however, would only describe the data over a very small temperature range. In contrast, Kaplan, Solomon, and Mott have developed a model based on the formation of long-lived spin pairs which predicts no explicit Zeeman splitting or temperature dependence.[22] While the latter model is assumed to apply to materials with long spin-lattice relaxation times T_1 such as C or Si the former should be more appropriate for materials with larger Z such as Ga or As. Neither model can account for the complicated temperature dependence in GaAs shown in Fig. 9.

Figure 10 shows the corresponding dependence of the Cr^{4+} EDMR signal amplitude on the microwave magnetic-field strength H_1. The *X*-band cavity used here provides a maximum magnetic field $H_1 = 2.3$ G at 2 W incident microwave power, as determined by electron-nuclear double resonance experiments[23] and standard electrodynamics.[24] Correspondingly, the *Q*-band cavity is expected to yield $H_1 = 1.5$ G at 250 mW incident microwave power. The EDMR amplitude exhibits a H_1-field dependence of $\Delta\sigma/\sigma \propto H_1^2$ at low microwave powers, followed by saturation at high powers. In contrast to conventional electron spin resonance, which has an amplitude proportional to the magnetization $M = \chi'' H_1$, the EDMR signal intensity is known to be proportional to the induced spin-flip rate or microwave power absorbed, $\Delta\sigma/\sigma \propto \chi'' H_1^2$,[25,26] as indeed observed at low-H_1 fields. The experimental data for the full H_1 dependence of $\Delta\sigma/\sigma$ in GaAs is best described by the behavior typical for homogeneous resonance lines in EDMR,

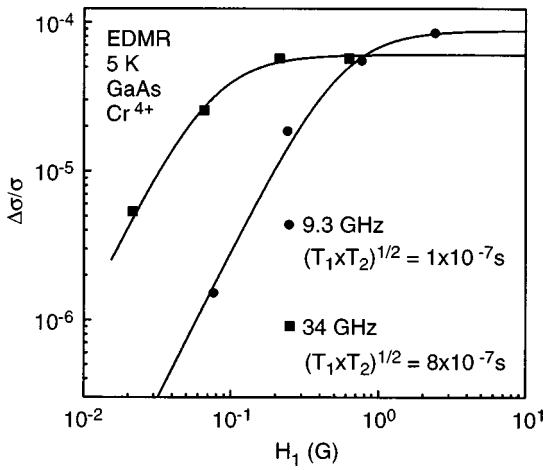

FIG. 10. Experimental and fitted power dependence of the Cr^{4+} EDMR signal amplitude for 9.3 nd 34 GHz. Within experimental error, $\Delta\sigma/\sigma$ is independent of the microwave frequency when saturation is reached.

$$\frac{\Delta\sigma}{\sigma} \propto \frac{T_2}{1+\gamma^2 H_1^2 T_1 T_2} H_1^2, \tag{3.3}$$

as shown by the fits in Fig. 10. The fits allow the estimation of $(T_1T_2)^{1/2}$ for the Cr^{4+} defect indicated in the figure. Due to the nuclear spins of Ga and As, the observed resonance lines are expected to be broadened by superhyperfine interactions. However, both the data shown here and similar results obtained on the power dependence of the the EDMR signal of As_{Ga} in neutron-irradiated GaAs,[27] are best described by Eq. (3.3) valid for homogeneously broadened lines. This discrepancy is probably caused by details of the EDMR process in GaAs, which remain to be investigated.

The EDMR temperature dependence shown in Fig. 9 can now be understood qualitatively. Increasing temperature leads to faster spin relaxation, shifting the power dependence of Fig. 10 to higher powers. As long as the saturation can still be reached with the microwave power available (i.e., the induced spin-flip rate is greater than the spontaneous spin-relaxation rate), only little change in the EDMR amplitude results, as seen in Fig. 9. However, when relaxation becomes so fast that no saturation can be reached, the amplitude of the EDMR signal is drastically reduced. The exact temperature dependence in this case will be determined by the temperature dependence of the spin relaxation, which can be very strong depending on the particular relaxation mechanism. This behavior poses a strong practical limitation on the temperature range relevant for EDMR measurements in GaAs: Using a conventional EPR spectrometer with typically 400 mW at 9 GHz and using moderate light intensities, EDMR experiments should be performed below 20 K. Higher powers or specific sample structures leading to a further enhancement of the H_1 field[28] could extend this range to temperatures better suited for the study of actual GaAs devices. Similarly, further reducing the light intensities so that T_1 is not governed by the carrier concentration could extend the temperature range. However, if the resistance R becomes too big, sensitivity is lost again according to Eq. (3.1).

The polarization model by Lepine predicts that the EDMR amplitude at saturation should be $\Delta\sigma/\sigma_{sat}=[g\mu_B H/(kT)]^2 \approx 10^{-2}$ at 5 K and 9.3 GHz. The fit in Fig. 10 provides an estimate for the experimentally observed amplitude $\Delta\sigma/\sigma_{sat}\approx 10^{-4}$. Further correcting according to Eq. (3.1) for the high modulation frequencies used, a maximum $\Delta\sigma/\sigma\approx 10^{-3}$ is found for the EDMR signal amplitude of Cr^{4+} in GaAs in our samples, still somewhat smaller then the value predicted by Lepine for 9.3 GHz. Since the temperature dependence of $\Delta\sigma/\sigma_{sat}$ is difficult to determine due to possible changes in the transport path and the limited microwave power as discussed above, the applicability of the Lepine model can only be tested by checking its prediction on the influence of the magnetic field H_0 or the microwave frequency ν on $\Delta\sigma/\sigma_{sat}$. Changing from 9.3 to 34 GHz should therefore increase $\Delta\sigma/\sigma_{sat}$ by a factor of $\approx$13. However, a quantitative comparison of EDMR experiments conducted on a single sample in both spectrometers, taking particular care that all experimental conditions including the illumination are identical apart from H_0 and ν, shows that within the experimental accuracy of at most 50%, $\Delta\sigma/\sigma_{sat}$ is independent of H_0 and ν, in clear contradiction to the Lepine model (Fig. 10). In fact, a similar lack of dependence of $\Delta\sigma/\sigma$ on H_0 and ν has been recently observed in a-Si:H using 434-MHz, 9.3- and 34-GHz spectrometers.[29] This suggests that both in Si and GaAs the Kaplan, Solomon, and Mott model invoking the formation of spin-pairs is the correct description of EDMR. However, for a complete understanding of the EDMR amplitude the influence of the defect concentration and possibly recombination times and capture cross sections need to be known, which could not be studied using the present samples.

IV. THE GALLIUM INTERSTITIAL

As already mentioned, the spin resonance spectra of the Ga interstitial are dominated by the hyperfine interaction with the nuclear spin of the Ga core. Since there are two stable isotopes, namely, ^{69}Ga and ^{71}Ga, both having a nuclear spin $I=3/2$, the Ga interstitial resonances shown in Figs. 3 and 12 are a superposition of two four-line spectra.

The general spin-Hamiltonian coupling the electronic spin **S** of a single Ga isotope to the nuclear spin **I** of the same isotope in a magnetic field **B** is

$$H=\mu_B \mathbf{S}\tilde{g}\mathbf{B}+\mathbf{S}\tilde{A}\mathbf{I}, \tag{4.1}$$

where μ_B is the Bohr magneton, **S** is the effective electron spin, $\tilde{g}$ the g tensor, **I** the nuclear spin, and $\tilde{A}$ the hyperfine tensor. The Ga interstitial resonances shown in Figs. 3 and 12 were found to be isotropic. Hence, both tensors $\tilde{g}$ as well as $\tilde{A}$ can be replaced by the scalars g and A, respectively. In the basis of vectors of the form $|m_S m_I\rangle$, the Hamiltonian (4.1) has the form

$$
\begin{array}{c}
 \\
\langle +\frac{1}{2}+\frac{3}{2}| \\
\langle +\frac{1}{2}+\frac{1}{2}| \\
\langle +\frac{1}{2}-\frac{1}{2}| \\
\langle +\frac{1}{2}-\frac{3}{2}| \\
\langle -\frac{1}{2}+\frac{3}{2}| \\
\langle -\frac{1}{2}+\frac{1}{2}| \\
\langle -\frac{1}{2}-\frac{1}{2}| \\
\langle -\frac{1}{2}-\frac{3}{2}|
\end{array}
\begin{array}{c}
\begin{array}{cccccccc}
|+\frac{1}{2}+\frac{3}{2}\rangle & |+\frac{1}{2}+\frac{3}{2}\rangle & |+\frac{1}{2}-\frac{3}{2}\rangle & |+\frac{1}{2}-\frac{3}{2}\rangle & |-\frac{1}{2}+\frac{3}{2}\rangle & |-\frac{1}{2}+\frac{3}{2}\rangle & |-\frac{1}{2}-\frac{3}{2}\rangle & |-\frac{1}{2}-\frac{3}{2}\rangle
\end{array} \\
\left(\begin{array}{cccccccc}
\frac{B}{2}(g\mu_B - 3g_n\mu_n) + \frac{3A}{4} & 0 & 0 & 0 & 0 & 0 & 0 & 0 \\
0 & \frac{B}{2}(g\mu_B - g_n\mu_n) + \frac{A}{4} & 0 & 0 & \frac{\sqrt{3}}{2}A & 0 & 0 & 0 \\
0 & 0 & \frac{B}{2}(g\mu_B + g_n\mu_n) - \frac{A}{4} & 0 & 0 & A & 0 & 0 \\
0 & 0 & 0 & \frac{B}{2}(g\mu_B + 3g_n\mu_n) - \frac{3A}{4} & 0 & 0 & \frac{\sqrt{3}}{2}A & 0 \\
0 & \frac{\sqrt{3}}{2}A & 0 & 0 & -\frac{B}{2}(g\mu_B + 3g_n\mu_n) - \frac{3A}{4} & 0 & 0 & 0 \\
0 & 0 & A & 0 & 0 & -\frac{B}{2}(g\mu_B + g_n\mu_n) - \frac{A}{4} & 0 & 0 \\
0 & 0 & 0 & \frac{\sqrt{3}}{2}A & 0 & 0 & -\frac{B}{2}(g\mu_B - g_n\mu_n) + \frac{A}{4} & 0 \\
0 & 0 & 0 & 0 & 0 & 0 & 0 & -\frac{B}{2}(g\mu_B - 3g_n\mu_n) + \frac{3A}{4}
\end{array}\right)
\end{array}
\tag{4.2}
$$

In the chosen representation the Zeeman term $g\mu_B\mathbf{SB}$ only contributes to the diagonal elements because with the magnetic field **B** along the z axis the scalar product between **S** and **B** involves only the z component of the spin operator **S** and the basis vectors $|m_S m_I\rangle$ of the Hamiltonian (4.2) are eigenvectors of S_z. The off-diagonal elements have their origin in the the hyperfine term $A\mathbf{SI}$, since the operators for x and y components of the effective spin **S** and nuclear spin **I** do not commute with the corresponding operators for the z component.

It can be assumed that the g values g for the ^{69}Ga interstitial and for the ^{71}Ga interstitial are identical because of the identical electronic properties of both isotopes. The hyperfine constants A_{69} and A_{71} on the other hand, should be different since the different core properties of the isotopes are involved via the nuclear spin **I**. The fact that an isotropic hyperfine interaction observed experimentally shows that the (isotropic) Fermi contact interaction is dominating and that the (anisotropic) dipolar interaction is negligible. The Fermi contact interaction is given

$$A_{69/71} = \frac{2\mu_0}{3} g\mu_B g_{n,69/71}\mu_n |\psi(0)|^2, \tag{4.3}$$

where $g_{n,69/71}$ and μ_n are the nuclear g factors of the Ga isotopes and the nuclear magneton, respectively.[30] $|\psi(0)|^2$ is the probability to find the paramagnetic electron at the nucleus. The nuclear g value of ^{69}Ga is $g_{n,69}=1.344$, that for ^{71}Ga is $g_{n,71}=1.708$. According to Eq. (4.3), the ratio of the hyperfine constants is then given by $A_{71}/A_{69}=g_{n,71}/g_{n,69}=1.27$.

A plot of the eigenvalues of Eq. (4.2) for the ^{69}Ga and ^{71}Ga interstitials as a function of the magnetic field (Breit-Rabi diagram) is shown in Fig. 11. For the calculations, $g=2.006$ and $A_{69}=0.048$ cm^{-1} have been used. Furthermore, the magnetic dipole transitions for microwave frequencies of 9.3 GHz and 34 GHz are included in the figure. They occur between eigenvalues whose corresponding eigenvectors are dominated by basis vectors $|m_S m_I\rangle$ with m_S changing by ± 1 and constant m_I.

The line positions for the X-band and Q-band EDMR as well as the Q-band ODMR investigations as determined from the Breit-Rabi diagram are indicated by vertical lines in Figs. 3 and 12, respectively, together with the experimental spectra. The Q-band EDMR spectrum has been obtained using the same phase shift analysis as described in the context of the X-band data above. The length of the bars is a measure of the relative intensities of the resonances as determined by the natural abundance ratio of ^{69}Ga and ^{71}Ga (40/60). The simulation including inhomogeneous broadening by Gaussian lines are in good agreement with the experimental EDMR and ODMR spectra.

Possible defects involving a single central Ga atom are the cation antisite Ga_{As} and the Ga interstitial Ga_i. The first possibility can be excluded because large cluster recursion calculations[31] do not find states in the gap for Ga_{As} and self-consistent Green's-function calculations[32] predicting a gap state with T_2 symmetry are inconsistent with the experimentally observed isotropic hyperfine interaction indicating an A_1 state. The Green's-function calculations[32] for the Ga_i, on the other hand, are consistent with the experimental findings since an A_1 gap state is predicted. Therefore, the spectra shown in Figs. 3 and 12 are assigned to the Ga interstitial.

There are three interstitial sites with high symmetry in the GaAs lattice. One has hexagonal (D_{3d}) and the two others have tetrahedral (T_d) symmetry. In contrast to the tetrahedral

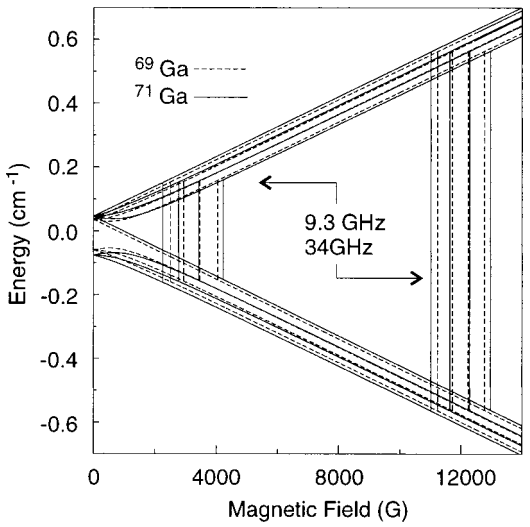

FIG. 11. Breit-Rabi diagram of the Ga_i and magnetic dipole transitions for X-band as well as Q-band frequencies ($g=2.006$, $A_{69}=0.048\ cm^{-1}$, and $A_{71}=0.061\ cm^{-1}$).

sites it seems to be very unlikely that the interstitial on the hexagonal site shows an isotropic Zeeman splitting. Therefore, the more likely candidates are the tetrahedral sites where the interstitial is surrounded by either four Ga or four As atoms. With Green's-function calculations[32] it has been shown that only the interstitial with As atoms in the nearest-neighbor shell has a paramagnetic state in the band gap; in this state the interstitial is two times positively charged (Ga_i^{2+}) and has therefore an effective spin $S=1/2$. The atomic structure of the Ga_i defect is shown in Fig. 13.

Table I lists the resonance parameters of the Ga interstitial in $Al_{0.4}Ga_{0.6}As$,[33,34] GaAs/AlAs superlattices,[35] and GaAs. The hyperfine constants are in agreement but the g value of the interstitial in $Al_{0.4}Ga_{0.6}As$ compared to the interstitials in the other two host materials is somewhat bigger. This difference in g factors implies that the electronic structure of the host material, seen by the interstitial, is similar in the superlattice and in our sample. This suggests that the interstitials in the codoped layer could be preferentially formed near to the interface. The isotropic hyperfine interaction of the interstitial in superlattices as well as in our codoped layer show that the defect wave function suffers no axial eccentricity due to the interface region—a fact that requires a strong localization of the wave function. The highly localized character is confirmed by the investigations of Kennedy and co-workers.[33,34] They show that for $Al_{0.4}Ga_{0.6}As$ the Ga_i resonance parameters are independent from the Al content. Hence, the interstitial does not see the atoms in the next-nearest-neighbor shell and the defect wave function must be highly localized.

V. CONCLUSIONS

We have shown that spin-dependent transport can be successfully extended to study defect properties in GaAs/$Al_{0.4}Ga_{0.6}As$ multilayer systems. Using electrically detected magnetic resonance, we have observed surface states and intrinsic defects, as well as a transition-metal impurity. Using different contact geometries and a phase shift analysis

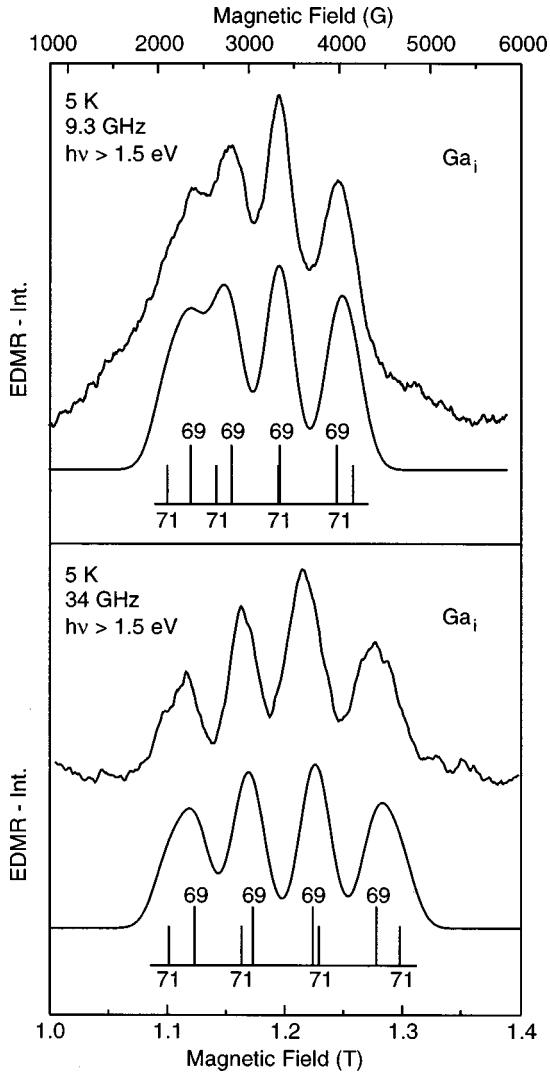

FIG. 12. Experimental and simulated X-band and Q-band EDMR spectra of the Ga_i ($g=2.006$, $A_{69}=0.048\ cm^{-1}$, and $A_{71}=0.061\ cm^{-1}$). The calculated line positions are indicated by vertical lines, proportional to the natural abundances of the Ga isotopes.

under illumination with inhomogeneously absorbed light, we have been able to determine the spatial location of the defects within the heterostructure. Two different models are discussed to quantitatively account for the signal size in

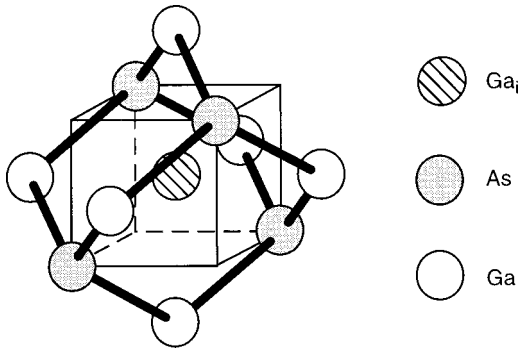

FIG. 13. Defect model of the Ga_i in GaAs. The Ga_i is located at a tetrahedral interstitial site with As atoms in the nearest and Ga atoms in the next-nearest-neighbor shell.

TABLE I. Defect parameters of the Ga interstitial in various host materials.

Material	g factor	A_{69} (cm^{-1})	A_{71} (cm^{-1})	Reference
$Al_xGa_{1-x}As$, $0.1 \leqslant x \leqslant 0.45$	2.025	0.050	0.064	33,34
GaAs/AlAs superlattice	2.007	0.054	0.069	35
GaAs	2.006	0.048	0.061	this work

EDMR. Our results demonstrate that electrically detected magnetic resonance has a much greater potential for the characterization of semiconductors with direct band gap than previously assumed.

ACKNOWLEDGMENT

This work was supported by the Deutsche Forschungsgemeinschaft (SFB 348).

[1] B. C. Cavenett, Adv. Phys. **57**, 475 (1981).
[2] J. Schmidt and I. Solomon, C. R. Acad. Sci. (France) **263**, 169 (1966).
[3] D. J. Lepine, Phys. Rev. B **6**, 436 (1972).
[4] J. Köhler, J. A. J. M. Disselhorst, M. C. J. M. Donckers, E. J. J. Groenen, J. Schmidt, and W. E. Moermer, Nature (London) **363**, 242 (1993).
[5] J. Wachtrup, C. von Borczyskowski, J. Bernard, M. Orrit, and R. Brown, Nature (London) **363**, 244 (1993).
[6] B. Henderson, M. Pepper, and R. L. Vranch, Semicond. Sci. Technol. **4**, 1045 (1989).
[7] I. Solomon, Solid State Commun. **20**, 215 (1976).
[8] N. M. Reinacher, M. S. Brandt, and M. Stutzmann, Mater. Sci. Forum **169-201**, 1915 (1995).
[9] N. M. Reinacher, M. S. Brandt, and M. Stutzmann, J. Appl. Phys. **80**, 4541 (1996).
[10] W. E. Carlos, E. R. Glaser, T. A. Kennedy, and S. Nakamura, Appl. Phys. Lett. **67**, 2376 (1995).
[11] Y. Mochizuki, M. Mizuta, and A. Mochizuki, Mater. Sci. Forum **196-201**, 1927 (1995).
[12] K. M. Lee, Rev. Sci. Instrum. **53**, 702 (1982).
[13] M. Godlewski, W. M. Chen, and B. Monemar, Mater. Sci. Forum **143-147**, 1353 (1994).
[14] T. A. Kennedy and N. D. Wilsey, Phys. Rev. B **32**, 6942 (1985).
[15] H. P. Gislason, F. Rong F, and G. D. Watkins, Phys. Rev. B **32**, 6945 (1985).
[16] P. Emanuelson, P. Omling, and B. K. Meyer, Mater. Sci. Forum **143-147**, 1541 (1994).
[17] U. Kaufmann and J. Schneider, Appl. Phys. Lett. **36**, 747 (1980).
[18] R. J. Wagner, J. J. Krebs, H. H. Stauss, and A. M. White, Solid State Commun. **36**, 15 (1980).
[19] E. A. Schiff, in *Tetrahedrally Bonded Amorphous Semiconductor*, edited by R. A. Street, D. K. Biegelsen, and J. C. Knights, AIP Conf. Proc. No. **73** (AIP, New York, 1981), p. 233.
[20] H. Dersch, L. Schweitzer, and J. Stuke, Phys. Rev. B **28**, 4678 (1983).
[21] B. K. Meyer and J.-M. Spaeth, J. Phys. C **18**, L99 (1985).
[22] D. Kaplan, I. Solomon, and N. F. Mott, J. Phys. (France) **39**, L51 (1978).
[23] M. Stutzmann and D. K. Biegelsen, Phys. Rev. B **34**, 3093 (1986).
[24] C. P. Poole, *Electron Spin Resonance* (Wiley, New York, 1983), Chap. 5.
[25] C. F. O. Graeff, M. Stutzmann, and M. S. Brandt, Phys. Rev. B **49**, 11 028 (1994).
[26] J. S. Hyde, Phys. Rev. **119**, 1492 (1960).
[27] N. M. Reinacher (unpublished).
[28] G. Kawachi, C. F. O. Graeff, M. S. Brandt, and M. Stutzmann, Jpn. J. Appl. Phys., Part 1 **36**, 121 (1997).
[29] M. S. Brandt, M. W. Bayerl, M. Stutzmann, and C. F. O. Graeff, J. Non-Cryst. Solids (to be published).
[30] E. Fermi, Z. Phys. **60**, 320 (1930).
[31] P. J. Lin-Chung and T. L. Reinecke, Phys. Rev. B **27**, 1101 (1983).
[32] G. A. Baraff and M. Schluter, Phys. Rev. Lett. **55**, 1327 (1985).
[33] T. A. Kennedy and M. G. Spencer, Phys. Rev. Lett. **57**, 2690 (1986).
[34] T. A. Kennedy, R. Magno, and M. G. Spencer, Phys. Rev. B **37**, 6325 (1988).
[35] J. M. Trombetta, T. A. Kennedy, W. Tseng, and D. Gammon, Phys. Rev. B **43**, 2458 (1991).